https://doi.org/10.5194/wes-2024-23
Preprint. Discussion started: 19 March 2024

eawe european academy of wind energy
Open Access WIND ENERGY SCIENCE DISCUSSIONS

A simple RANS inflow model of the neutral and stable atmospheric boundary layer applied to wind turbine wake simulations

Maarten Paul van der Laan[1], Mark Kelly[1], Mads Baungaard[1], and Antariksh Dicholkar[1]

[1]Technical University of Denmark, DTU Wind and Energy Systems, Risø Campus, Frederiksborgvej 399, 4000 Roskilde, Denmark

Correspondence: Maarten Paul van der Laan (plaa@dtu.dk)

Abstract. Wind turbines are increasing in size and operate more frequently above the atmospheric surface layer, which requires improved inflow models for numerical simulations of turbine interaction. In this work, a steady-state Reynolds-averaged Navier-Stokes (RANS) model of the neutral and stable atmospheric boundary layer (ABL) is introduced. The model employs a buoyancy source using a prescribed Brunt-Väisälä frequency, does not require a global turbulence length scale limiter, and is only dependent on two non-dimensional numbers. The proposed model assumes a constant temperature gradient over the entire ABL, which is a strong assumption but leads to a simple and well behaving inflow model. RANS wake simulations subjected to shallow and tall ABLs are performed and the results show a good agreement with results from two different large-eddy simulation codes in terms of velocity deficit.

1 Introduction

Wind turbine and farm interaction can lead to energy losses and increased turbine loads, mainly due to wakes from upstream turbines and farms, but also because of blockage effects (Porté-Agel et al., 2020). The magnitude of these effects is strongly influenced by the atmospheric conditions as ambient turbulence intensity (Nilsson et al., 2015), buoyancy and boundary layer depth (Hansen et al., 2012). Traditionally, models for simulating wake losses assume simple atmospheric conditions that only represent the first 10% of the atmospheric boundary layer (ABL), known as the atmospheric surface layer (ASL). Examples are wind speed profiles based on a power law or Monin-Obukhov Similarity Theory (Monin and Obukhov, 1954). However, wind turbines are increasing in size and operate more frequently above the ASL, especially for shallow ABLs. Hence, there is a need for improved inflow models that can capture the effect of the ABL on the wind farm flow.

Wind farm flow models based on Computational Fluid Dynamics (CFD) can be employed to simulate wake losses (Porté-Agel et al., 2020). High-fidelity turbulence-resolving and transient CFD methods as large-eddy simulation (LES) is a popular method in academia because it can simulate the complex interaction between the ABL and a wind farm; however, it is too expensive to simulate all wind direction and wind speed flow cases that are necessary to calculate wake losses in terms of annual energy production (AEP). For the latter, the industry employs engineering wake models because of their computational speed. However, such models require calibration and are often not general enough to perform well for a wide range of atmospheric conditions and wind farm layouts due to the need for assuming a single wake shape and wake superposition method. Reynolds-

https://doi.org/10.5194/wes-2024-23
Preprint. Discussion started: 19 March 2024

averaged Navier-Stokes (RANS) is a medium-fidelity steady-state CFD method that is several orders of magnitude faster than LES and does not require the engineering wake model assumptions. An idealized RANS setup of a large wind farm (16×16 turbines with $8D$ inter spacing) can simulate AEP wake losses in roughly a day using 624 CPUs (van der Laan et al., 2022). However, RANS requires a turbulence model, which is not trivial but reasonable results in terms of velocity and power deficits can be achieved (Politis et al., 2012; van der Laan et al., 2015c, b; Baungaard et al., 2022). In addition, atmospheric inflow modeling in RANS is challenging because the inflow needs to be a solution of the RANS model and numerical convergence is not guaranteed when ABL models beyond the neutral ASL are employed as an inflow model to wind farm simulations (van der Laan et al., 2023b).

Steady-state inflow models of the ABL often rely on the global length scale limiter of Apsley and Castro (1997), where a maximum turbulence length scale is chosen that indirectly determines the ABL height. When such an inflow model is applied to a 3D RANS simulation (Koblitz et al., 2015; van der Laan et al., 2015a; Avila et al., 2017), as for example a wind farm or complex terrain, then all turbulence length scales will also be limited, which can result in non physical solutions. In previous work (van der Laan et al., 2023b), an alternative ABL inflow model was proposed, where the global turbulence length scale limiter of Apsley and Castro (1997) was replaced by a turbulent buoyancy source with a prescribed potential temperature profile representing conventionally neutral ABLs. This model works well for tall ABLs but it is less suited to model shallow ABLs, which is shown in Appendix A. In the present work, a new ABL inflow model is proposed that does not require a global length scale limiter and is also suited to model shallow (and stable) ABLs. The model employs a turbulent buoyancy source that depends on a prescribed Brunt-Väisälä frequency by assuming a constant temperature gradient over the entire ABL. While this is a strong assumption, the resulting model is simple and well behaving. In addition, the proposed model can simulate the effect of neutral and stable atmospheric conditions on a wind turbine wake in RANS. The two existing and the proposed RANS inflow models are discussed in detail in Sect. 2 The three RANS inflow models are employed to single wake simulations following a methodology described in Sect. 3, and the results are compared with results of LES in Sect. 4, for both a shallow and a tall ABL.

2 RANS inflow models of the ABL

RANS inflow models of the ABL are based on a numerical solution of the 1D momentum equations, for streamwise and lateral velocity components, U and V, respectively, including a prescribed pressure gradient in the form of a geostrophic wind speed, $G = \sqrt{U_G^2 + V_G^2}$, and Coriolis forces. Here, U_G and V_G are the streamwise and lateral component of geostrophic wind vector. The momentum equations only depend on a single Cartesian coordinate, namely, the vertical coordinate, z:

$$f_c(V - V_G) + \frac{d}{dz}\left(\nu_T \frac{dU}{dz}\right) = 0, \qquad -f_c(U - U_G) + \frac{d}{dz}\left(\nu_T \frac{dV}{dz}\right) = 0, \tag{1}$$

with f_c as the Coriolis parameter. In addition, we have employed the Boussinesq hypothesis with ν_T as the eddy viscosity for which a turbulence model is required. In the present work, we use the k-ε-f_P eddy viscosity model (van der Laan et al., 2015c)

https://doi.org/10.5194/wes-2024-23
Preprint. Discussion started: 19 March 2024

eawe european academy of wind energy
Open Access WIND ENERGY SCIENCE DISCUSSIONS

that employs a transport equation for both the turbulent kinetic energy, k, and its dissipation, ε:

$$\nu_T = C_\mu f_P \frac{k^2}{\varepsilon}, \tag{2}$$
$$\frac{d}{dz}\left(\frac{\nu_T}{\sigma_k}\frac{dk}{dz}\right) + \mathcal{P} - \varepsilon + \mathcal{B} + S_{k,\mathrm{amb}} = 0, \qquad \frac{d}{dz}\left(\frac{\nu_T}{\sigma_\varepsilon}\frac{d\varepsilon}{dz}\right) + \left(C^*_{\varepsilon,1}\mathcal{P} - C_{\varepsilon,2}\varepsilon + C_{\varepsilon,3}\mathcal{B}\right)\frac{\varepsilon}{k} + S_{\varepsilon,\mathrm{amb}} = 0,$$

with f_P as a scalar function that acts as a local turbulence length scale limiter in regions with high velocity gradients to assure realizable Reynolds stresses, which is mainly applicable to a wind turbine (near) wake. However, f_P is not of importance to an inflow model but applied to be consistent with a 3D RANS simulation of a wind turbine wake. Furthermore, $\mathcal{P}$ and $\mathcal{B}$ are the turbulent production due to shear and buoyancy, respectively:

$$\mathcal{P} = \nu_T\left[\left(\frac{dU}{dz}\right)^2 + \left(\frac{dV}{dz}\right)^2\right], \qquad \mathcal{B} = \frac{g}{\theta_0}\overline{\theta' w'} = -\frac{\nu_T}{\sigma_\theta}\frac{g}{\theta_0}\frac{d\Theta}{dz}, \tag{3}$$

with $g = 9.81$ ms^{-2} as the magnitude of the gravitational acceleration vector, Θ as the mean potential temperature with θ_0 as the hydrostatic background temperature (here we use the value at the wall boundary), and a simple flux-gradient relationship for the heat flux, $\overline{\theta' w'} = -(\nu_T/\sigma_\theta)d\Theta/dz$, is employed. Note that in order to obtain a steady-state solution of the ABL, one cannot employ an active temperature equation in combination with a non-linear temperature profile, as such a setup would effectively become an unsteady RANS method due to a forever growing ABL height. $S_{k,\mathrm{amb}}$ and $S_{\varepsilon,\mathrm{amb}}$ are additional source terms used to maintain a small ambient value of turbulence for numerical robustness such that $k = k_{\mathrm{amb}}$ and $\varepsilon = \varepsilon_{\mathrm{amb}}$ in absence of any velocity gradients, applicable to the flow above the ABL (van der Laan et al., 2015a):

$$S_{k,\mathrm{amb}} = \varepsilon_{\mathrm{amb}}, \qquad S_{\varepsilon,\mathrm{amb}} = C_{\varepsilon,2}\frac{\varepsilon^2_{\mathrm{amb}}}{k_{\mathrm{amb}}}, \qquad k_{\mathrm{amb}} = \frac{3}{2}G^2 I^2_{\mathrm{amb}}, \qquad \varepsilon_{\mathrm{amb}} = C_\mu^{3/4}\frac{k^{3/2}_{\mathrm{amb}}}{\ell_{\mathrm{amb}}}, \tag{4}$$

with ℓ_{amb} and I_{amb}, as the ambient turbulence length scale and turbulence intensity (based on k) above the ABL, respectively, and C_{amb} as a model constant (van der Laan et al., 2020). The values of I_{amb} and C_{amb} are set small enough to not influence the inflow model solution. Furthermore, the definition of ℓ_{amb} differs with the chosen inflow model and is discussed in Sects. 2.1-2.3. In addition, the following turbulence model constants are used: $(C_\mu, C_{\varepsilon,1}, C_{\varepsilon,2}, \sigma_k, \sigma_\varepsilon, \sigma_\theta) = (0.03, 1.21, 1.92, 1.0, 1.3, 0.74)$, and turbulence model parameters $C^*_{\varepsilon,1}$ and $C_{\varepsilon,3}$ are also discussed in Sects. 2.1-2.3.

2.1 RANS-ℓ_{max}: Inflow model using the turbulence length scale limiter of Apsley and Castro (1997)

The global turbulence length scale limiter of Apsley and Castro (1997) can be employed to model a neutral and a stable inflow model without the need for turbulent buoyancy source term ($\mathcal{B} = 0$). The limiter represents a variable $C^*_{\varepsilon,1}$ in the transport equations of ε:

$$C^*_{\varepsilon,1} = C_{\varepsilon,1} + (C_{\varepsilon,2} - C_{\varepsilon,1})\frac{\ell}{\ell_{\mathrm{max}}} \tag{5}$$

where $\ell \equiv C_\mu^{3/4}k^{3/2}/\varepsilon$ is a model-based turbulence length scale. When ℓ exceeds ℓ_{max} then the source terms in the ε equation cancel and this prevents the turbulence length scale from growing larger than the maximum set value, ℓ_{max}. The height of the

https://doi.org/10.5194/wes-2024-23
Preprint. Discussion started: 19 March 2024

eawe european academy of wind energy
Open Access WIND ENERGY SCIENCE DISCUSSIONS

ABL can be set implicitly using $\ell_{\max}$. For $\ell_{\max} \to 0$ and $\ell_{\max} \to \infty$, the analytic ABL solutions of Ekman (1905) (constant ν_T) and Ellison (1956) (linear ν_T with z) are obtained, respectively, which bounds the numerical RANS model, as shown in van der Laan et al. (2020). When the global turbulence length scale limiter of Apsley and Castro (1997) is applied as an inflow model to a 3D RANS simulation, then all turbulence length scales are limited and this can lead to a non-physical recovery of a wake generated by for example a wind turbine, a wind farm or a hill (Koblitz et al., 2015; van der Laan et al., 2015a; Avila et al., 2017). An ad-hoc solution has been proposed in previous work (van der Laan et al., 2015a) by switching off the turbulence length scale limiter in wake region using the f_P function as a wake identifier:

$$C^*_{\varepsilon,1} = f_1 \left[C_{\varepsilon,1} + (C_{\varepsilon,2} - C_{\varepsilon,1}) \frac{\ell}{\ell_{\max}} \right], \qquad f_1 = \frac{1}{2} \left[\tanh \left(50 \left[f_P - 0.9 \right] \right) + 1 \right] \tag{6}$$

Here, f_1 is a blending function that switches between the global ($\ell_{\max}$) and local (f_P) turbulence length scale limiters. The impact of this solution on a single wake is further investigated in Sect. 4. The ambient values of k and ε are set by Eq. (4), where the ambient turbulence length scale is defined as:

$$\ell_{\text{amb}} = C_{\text{amb}} \ell_{\max} \tag{7}$$

with $C_{\text{amb}} = 10^{-6}$ and $I_{\text{amb}} = 10^{-6}$ (van der Laan et al., 2020). We label the inflow model as the RANS-$\ell_{\max}$ model.

2.2 RANS-Θ: Prescribed temperature inflow model

The RANS-$\ell_{\max}$ can lead to non-physical wake recovery when it is applied as an inflow model to wind farm, especially for shallow ABLs. To overcome this issue, an alternative RANS inflow model has recently been developed (van der Laan et al., 2023b), here labeled as the RANS-Θ model, where the global length scale limiter of Apsley and Castro (1997) has been replaced ($C^*_{\varepsilon,1} = C_{\varepsilon,1}$) by the use of a non-zero turbulence buoyancy from Eq. (3), and an analytic prescribed temperature profile that includes a constant temperature in the surface layer and a constant inversion:

$$\frac{d\Theta}{dz} = \frac{1}{2} \left[1 + \tanh \left(\frac{z/z_i - 1}{z_T/z_i} \right) \right] \left. \frac{d\Theta}{dz} \right|_c, \tag{8}$$

where z_i as the inversion height, $d\Theta/dz|_c$ is the inversion strength, and z_T characterizes the fraction of z_i over which the temperature gradient changes from 0 to $d\Theta/dz|_c$ (we take $z_T/z_i = 0.2$). The temperature profile can be obtained upon integration and its final form is described in van der Laan et al. (2023b). The temperature profile remains constant when the model is applied as inflow to a 3D RANS simulation, since $\Theta(z)$ from (8) is prescribed instead of solving a temperature equation. Note that the original RANS-θ model was employed with a slightly different implementation of the buoyancy compared to Eq. (3), namely, $\mathcal{B} = -(\nu_T/\sigma_\theta)(g/\Theta) d\Theta/dz$. However, $\Theta \simeq \theta_0$, since $z_i d\Theta/dz|_c \ll \theta_0$ for the values of z_i and $d\Theta/dz|_c$ encountered in the ABL (here, we use the wall temperature to represent the hydrostatic temperature θ_0).

The ambient turbulence length scale above the ABL is defined as:

$$\ell_{\text{amb}} = C_{\text{amb}} z_i. \tag{9}$$

https://doi.org/10.5194/wes-2024-23
Preprint. Discussion started: 19 March 2024

eawe european academy of wind energy
Open Access WIND ENERGY SCIENCE DISCUSSIONS

In addition, we use $I_{\text{amb}} = 10^{-5}$ and $C_{\text{amb}} = 10^{-7}$. Finally, the $C_{\varepsilon,3}$ constant is defined as

$$C_{\varepsilon,3} = 1 + C_{\varepsilon,1} - C_{\varepsilon,2} \tag{10}$$

following Sogachev et al. (2012) for $\ell_{\max} \to \infty$.

The RANS-Θ model is suited to model a conventionally neutral ABL (CNBL). However, if one selects an inconsistent combination of z_i and $d\Theta/dz|_c$ then an unphysical inflow profile (with effectively two ABL heights) can result. This problem is further illustrated in Appendix A for a (too) shallow ABL.

2.3 RANS-N: New inflow model based on a constant Brunt-Väisälä frequency

The buoyant destruction of turbulent kinetic energy from (3) can be written as

$$\mathcal{B} = -\frac{\nu_T}{\sigma_\theta}\frac{g}{\theta_0}\frac{d\Theta}{dz} = -\frac{\nu_T}{\sigma_\theta}N^2, \tag{11}$$

where the Brunt-Väisälä frequency is described by

$$N \equiv \sqrt{\frac{g}{\theta_0}\frac{d\Theta}{dz}}. \tag{12}$$

The problems with the RANS-$\ell_{\max}$ and RANS-Θ models outlined above can be overcome by prescribing a constant gradient of temperature throughout the entire ABL in (11), giving a constant $N \to N_{\text{ABL}}$ in (12). The turbulence model constant σ_θ (turbulent Prandtl number) is set to one for simplicity, as it could be absorbed in N_{ABL}. The RANS-Θ model can also be written in the form of (11), but with a vertically varying temperature gradient and $N(z)$, where as $z \to z_i$ in the upper ABL $d\Theta/dz \to (d\Theta/dz)|_c$ and $N \to N_c$. The simple form of $\mathcal{B}$ with a constant N also implies that the heat flux profile is same as the eddy viscosity profile times a constant, $\overline{\theta' w'} = -N^2(\theta_0/[g\sigma_\theta])\nu_T$. A constant temperature gradient was also assumed by Chougule et al. (2017) to simulate atmospheric boundary turbulence with a spectral tensor model including effects of buoyancy. Using a constant N or constant temperature gradient for the entire ABL is not always realistic, but this model choice results in a simple RANS ABL inflow model, which we label the RANS-N model, that can yield reasonable results of the ABL; this is further discussed in Sect. 4. Furthermore, the RANS-N model does not suffer from the "double" ABL height problem that can occur with the RANS-Θ model, because the RANS-N model does not require an explicit inversion height. The RANS-N model behaves similarly to the RANS-$\ell_{\max}$ model in terms of obtaining an ABL height implicitly using a single parameter; instead of an ABL length scale arising from $\ell_{\max}$ (i.e. $z_i \simeq \ell_{\max}^{0.6}(G/f)^{0.4}$ as in van der Laan et al., 2020), the depth is determined by the constant N_{ABL}. We note that one can also translate N_{ABL} to an ABL length scale using G/N_{ABL}. The latter defines an ambient turbulence length scale above the ABL:

$$\ell_{\text{amb}} = C_{\text{amb}}\frac{G}{N_{\text{ABL}}}, \tag{13}$$

with $C_{\text{amb}} = 10^{-7}$ and $I_{\text{amb}} = 10^{-5}$. If $N_{\text{ABL}} = 0$, then ε_{amb} is set to zero. Since the RANS-N model does not use the global length scale limiter of Apsley and Castro (1997) ($C^*_{\varepsilon,1} = C_{\varepsilon,1}$), the model does not artificially limit the turbulence length scale in a 3D RANS simulation. The remaining constant, $C_{\varepsilon,3}$, is set the same as the RANS-Θ model (Eq. 10).

https://doi.org/10.5194/wes-2024-23
Preprint. Discussion started: 19 March 2024

eawe european academy of wind energy
Open Access WIND ENERGY SCIENCE DISCUSSIONS

2.4 Similarity

The RANS ABL models discussed here ultimately depend on four or five dimensional parameters, but their non-dimensional numerical solutions can be described by two or three dimensionless numbers (following the Buckingham-Pi theorem), as summarized in Table 1. The first dimensionless number is the surface Rossby number, $\mathrm{Ro}_0 \equiv G/(|f_c|z_0)$, and can be obtained

Model	Dimensional input	Non-dimensional input
RANS-$\ell_{\max}$	G, f_c, z_0, $\ell_{\max}$	Ro_0, Ro_ℓ
RANS-Θ	G, f_c, z_0, z_i, $\frac{d\Theta}{dz}\big\vert_c$, θ_0	Ro_0, Ro_{z_i}, N_f
RANS-N	G, f_c, z_0, N_{ABL}	Ro_0, N_f

Table 1. Dimensional and non-dimensional input parameters of RANS inflow models.

by writing the 1D momentum equations (Eq. 1) in a complex form using $W \equiv (U-U_G)+i(V-V_G)$, with $i \equiv \sqrt{-1}$, followed by a substitution of the normalized variables, $z' \equiv z/z_0$, $W' \equiv W/G$ and $\nu_T' \equiv \nu_T/(z_0 G)$:

$$\mathrm{Ro}_0 \frac{d}{dz'}\left(\nu_T' \frac{dW'}{dz'}\right) = iW'. \tag{14}$$

All models that solve the momentum equation (14) follow a Rossby similarity. The other dimensionless numbers are related to the turbulence model equations (2), which can be written in a non-dimensional form using $k' = k/G^2$, $\varepsilon' = \varepsilon z_0/G^3$:

$$\begin{aligned} &\frac{d}{dz'}\left(\frac{\nu_T'}{\sigma_k}\frac{dk'}{dz'}\right) + \mathcal{P}' + \mathcal{B}' - \varepsilon' = 0, \\ &\frac{d}{dz'}\left(\frac{\nu_T'}{\sigma_\varepsilon}\frac{d\varepsilon'}{dz'}\right) + \left(C_{\varepsilon,1}^* \mathcal{P}' - C_{\varepsilon,2}\varepsilon' + C_{\varepsilon,3}\mathcal{B}'\right)\frac{\varepsilon'}{k'} = 0, \end{aligned} \tag{15}$$

with $\mathcal{P}' \equiv \mathcal{P} z_0/G^3$ and $\mathcal{B}' \equiv \mathcal{B} z_0/G^3$. Here, the small ambient source terms are neglected. The additional dimensionless numbers are obtained from non-dimensionalizing either $C_{\varepsilon,1}^*$ (Eq. 5) or $\mathcal{B}'$ (via Eqns. 3, 8, 11):

$$\begin{aligned} &\mathrm{RANS}{-}\ell_{\max}: \quad \mathcal{B}' = 0, && C_{\varepsilon,1}^* = C_{\varepsilon,1} + (C_{\varepsilon,2} - C_{\varepsilon,1})\, C_\mu^{3/4} \tfrac{k'^{3/2}}{\varepsilon'} \tfrac{\mathrm{Ro}_\ell}{\mathrm{Ro}_0}, \\ &\mathrm{RANS}{-}\Theta: \quad \mathcal{B}' = -\tfrac{\nu_T'}{\sigma_\theta}\left(\tfrac{\mathrm{N}_f}{\mathrm{Ro}_0}\right)^2 \left[\tfrac{1}{2} + \tfrac{1}{2}\tanh\left(\tfrac{z'\mathrm{Ro}_{z_i}/\mathrm{Ro}_0 - 1}{z_T/z_i}\right)\right], && C_{\varepsilon,1}^* = C_{\varepsilon,1}, \\ &\mathrm{RANS}{-}N: \quad \mathcal{B}' = -\tfrac{\nu_T'}{\sigma_\theta}\left(\tfrac{\mathrm{N}_f}{\mathrm{Ro}_0}\right)^2, && C_{\varepsilon,1}^* = C_{\varepsilon,1}, \end{aligned} \tag{16}$$

where $\mathrm{Ro}_\ell \equiv G/(|f_c|\ell_{\max})$ and $\mathrm{Ro}_{z_i} \equiv G/(|f_c|z_i)$ are Rossby numbers based on different ABL length scales, namely, $\ell_{\max}$ and z_i, respectively. In addition, $\mathrm{N}_f \equiv N/|f_c|$ is the Zilitinkevich number using the Brunt-Väisälä frequency from Eq. (12) using a constant gradient of temperature (representing the inversion or the entire ABL for the RANS-Θ and RANS-N models, respectively). Note that one could also replace N_f by a Richardson number, in the form of $(\mathrm{N}_f/\mathrm{Ro}_0)^2$. The similarity of the RANS-$\ell_{\max}$ and RANS-Θ models has been shown through numerical experiments in previous work (van der Laan et al., 2020, 2023b). The similarity of the ABL models can be employed to create an ABL library numerically for all possible solutions, which can be used to obtain an ABL profile with a desired turbulence intensity and wind speed at a reference height

https://doi.org/10.5194/wes-2024-23
Preprint. Discussion started: 19 March 2024

eawe european academy of wind energy
Open Access WIND ENERGY SCIENCE DISCUSSIONS

by using G and N_{ABL} (in the case of the RANS-N model) as free parameters, for a given f_c and z_0. The proposed RANS-N model has one fewer dimensional number compared to the RANS-Θ model, which reduces the input parameter space.[1] In addition, all three RANS models can be used to satisfy Reynolds number similarity by keeping their non-dimensional numbers constant. This is an advantage when running wind speed inflow cases consecutively to reduce the total number of required iterations for wind farm AEP simulations (van der Laan et al., 2019, 2022).

3 Numerical methodology

The RANS simulations of the inflow and single turbine wake are carried out with PyWakeEllipSys (DTU Wind and Energy Systems, 2024), which is Python framework for wind farm CFD simulations. The underlying CFD solver is EllipSys; which is an in-house finite volume code initially developed by Michelsen (1992); Sørensen (1994). The numerical domain and boundary conditions of the 1D inflow precursor and 3D wind turbine simulations are depicted in Fig. 1, and are further discussed in Sects. 3.1 and 3.2.

3.1 Inflow

The RANS inflow models are solved numerically with EllipSys1D (van der Laan and Sørensen, 2017). A 1D grid with a height of 100 km, a first cell height of 0.01 m and 768 cells are employed, as shown in Fig. 1a. A relative tall domain is employed to be able to simulate all possible ABL solutions. A rough wall boundary condition from Sørensen et al. (2007) is employed at the ground, and depends on the roughness length z_0. At the top, a Neumann condition is applied. Since the 1D RANS equations are stiff, we solve them transient with a fixed time step of $\Delta t = 1/f_c$ until a steady-state has been achieved.

3.2 Single wake

The RANS inflow models are applied to RANS single wake simulations, performed with EllipSys3D. The numerical setup follows a very similar approach as performed in previous work (van der Laan et al., 2015c) and solves the three-dimensional form of Eqns. (1-2). We aim to compare the RANS simulations (both inflow and single wake) with results of two LES models from Hodgson et al. (2023). These LES models employ an Actuator Disk (AD) model based on airfoil data to represent the forces of the SWT-2.3-93 turbine, which has a rated power of 2.3 MW, a rotor diameter, D, of 93 m, and a hub height, z_H, of 68.5 m. Our RANS simulations use the same turbine type, but we employ an AD (Réthoré et al., 2014) including the analytic blade force distribution model of Sørensen et al. (2020), which has shown to compare well with an AD based on airfoil data. This AD model includes effects of rotor rotation and non-uniform inflow as wind shear and wind veer. In addition, we use a 1D momentum controller (Calaf et al., 2010) similar to one of LES models from Hodgson et al. (2023), based on the same inputs: a tip speed ratio of 7.75 and a thrust coefficient of 0.73 and a power coefficient of 0.45. The actual values can differ

[1] It could appear that the RANS-Θ model further includes the parameter z_T, but this may be eliminated by relating N_{ABL} to $N(z)$ and N_c following Kelly et al. (2019); however this is beyond the scope of the current work.

https://doi.org/10.5194/wes-2024-23
Preprint. Discussion started: 19 March 2024

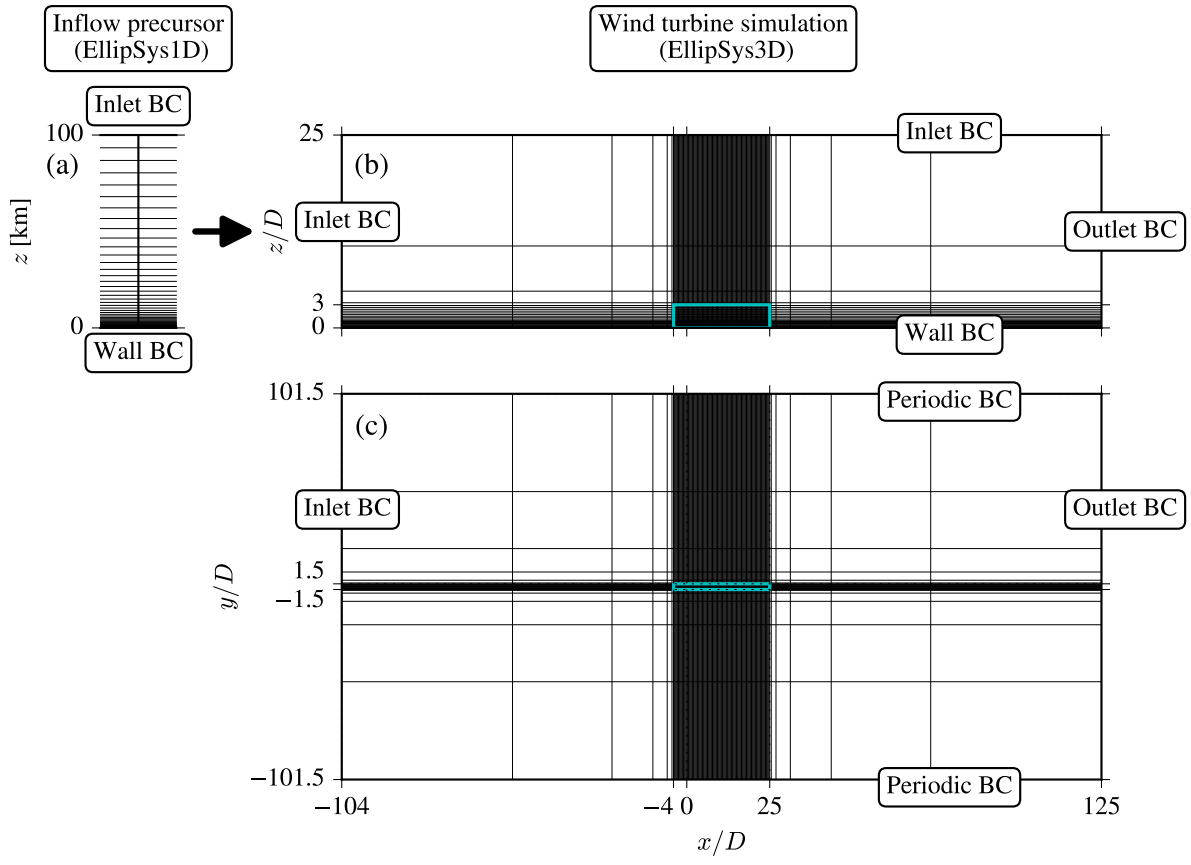

Figure 1. Numerical grid and boundary conditions of the 1D inflow precursor **(a)** and 3D wind turbine simulations **(b-c)**. Cyan rectangle marks the refined domain around the turbine and every 8th cells is shown.

because a 1D momentum controller typically overestimates the freestream wind speed and thrust force, as shown in previous work (van der Laan et al., 2015b), but we apply this controller to be consistent with the LES data.

A Cartesian domain is employed with dimensions $229D \times 203D \times 25D$ for the streamwise (x), lateral (y) and vertical (z) directions, respectively, as depicted in Fig. 1a-b. The large domain extend is used to minimize the effect of numerical blockage. An inner domain around the turbine, located at $(x, y, z) = (0, 0, z_H)$, is used to resolve the wind turbine wake with a fine uniform spacing of $D/32$ (cyan rectangle in Fig. 1a-b). The inner domain has the following horizontal dimensions: $-4D < x < 25D$ and $-1.5D < y < 1.5D$. Vertically, the cell sizes are growing with z using a first cell height of $D/200$, a maximum cell size of $D/32$ at $z = 3D$ and a maximum expansion ratio of 1.2. Above $z = 3D$, the cells continue to grow with a similar expansion ratio. The total number of cells is 37.7 million. The effect of coarser grid spacing is shown in Appendix B. An inlet boundary condition is at the inflow boundary ($x = -104D$) and at the top of domain ($z = 25D$). The bottom boundary is a rough wall boundary condition (Sørensen et al., 2007). The lateral boundaries ($y = \pm 101.5D$) are periodic because of the presence of wind veer. A Neumann condition is set at the outflow boundary ($x = 125D$). More details of the numerical setup

https://doi.org/10.5194/wes-2024-23
Preprint. Discussion started: 19 March 2024

eawe european academy of wind energy
Open Access WIND ENERGY SCIENCE DISCUSSIONS

are discussed in van der Laan et al. (2015c). with the exception of the lateral boundaries, which are set to periodic boundary conditions because of the presence of wind veer.

4 Results and discussion: A comparison with LES

4.1 Inflow

The two existing and proposed RANS inflow models from Sect 2 are applied to two ABL cases based on LES results from Hodgson et al. (2023), who used two different LES models. The ABL cases represent a CNBL and a stable ABL (SBL) inspired by LES inter-comparison study from Beare et al. (2006). The LES models from Hodgson et al. (2023) are employed with $f_c = 1.185 \times 10^{-4}$ s^{-1} and $z_0 = 0.001$ m. The values of the Coriolis parameter corresponds to a latitude of 54.3° and it is based on the location of the Danish offshore wind farm, Rødsand II. While we adopt the value of f_c from Hodgson et al. (2023), a lower roughness length is used in the RANS models. This is because the RANS models use $C_\mu = 0.03$ while LES models indicate a higher C_μ based on the turbulent kinetic energy and friction velocity near the wall, as shown in Baungaard et al. (2024). This is compensated by using a lower roughness length of $z_0 = 0.0002$ m in RANS-$\ell_{\max}$ and RANS-N models. Note if a higher C_μ would be set in the RANS models then the other turbulence model constants need to adjusted and calibrated, which is not the scope of the present article. The RANS inflow models use G and an additional parameter to obtain the turbulence intensity based on k, I_H, and wind speed, U_H, at the reference height of 68.5 m, namely, $\ell_{\max}$, z_0 and N_{ABL} for RANS-$\ell_{\max}$, RANS-Θ and RANS-N, respectively. The LES-derived input parameters and fitted RANS inflow model parameters are listed in Table 2. The RANS-$\ell_{\max}$ and RANS-N models use pre-calculated libraries of all possible ABL solutions that depend on two non-dimensional numbers (as discussed in Sect. 2.4), to look up the values for G and an ABL scale ($\ell_{\max}$ or N_{ABL}), for a given set of I_H and U_H. The RANS-Θ model uses an optimizer to find the values of G and z_0 for the CNBL case. LES-diagnosed values of θ_0, z_i and $d\Theta/dz|_c$ are not necessary for the SBL case because we do not employ the RANS-Θ model for this case.

	LES-derived input					RANS-$\ell_{\max}$		RANS-Θ		RANS-N	
	I_H	U_H	θ_0	z_i	$d\Theta/dz\|_c$	G	$\ell_{\max}$	G	z_0	G	N_{ABL}
Case	[%]	[ms^{-1}]	[K]	[m]	[Km^{-1}]	[ms^{-1}]	[m]	[ms^{-1}]	[m]	[ms^{-1}]	[s^{-1}]
CNBL	5.3	8.4	277.3	650	3.75×10^{-3}	9.67	30.7	9.31	9.31×10^{-5}	9.56	3.90×10^{-3}
SBL	3.1	8.8	-	-	-	9.58	3.38	-	-	9.85	2.71×10^{-2}

Table 2. LES-derived input from ABL cases and fitted parameters of RANS inflow models.

The RANS inflow model results are compared with the two LES models from Hodgson et al. (2023), for the CNBL and SBL cases in Fig. 2. The result of the LES models compare well with the results of the RANS-$\ell_{\max}$ and RANS-N models in terms of wind speed and turbulence intensity based on k, for both ABL cases (Fig. 2a, c, g and i). The good fit around hub height is expected since the RANS models are tuned for the LES-predicted values of I_H and U_H. The main difference between the models are the profiles of turbulence length scale (Fig. 2d,j) and eddy viscosity (Fig. 2e and k), where the RANS-$\ell_{\max}$

https://doi.org/10.5194/wes-2024-23
Preprint. Discussion started: 19 March 2024

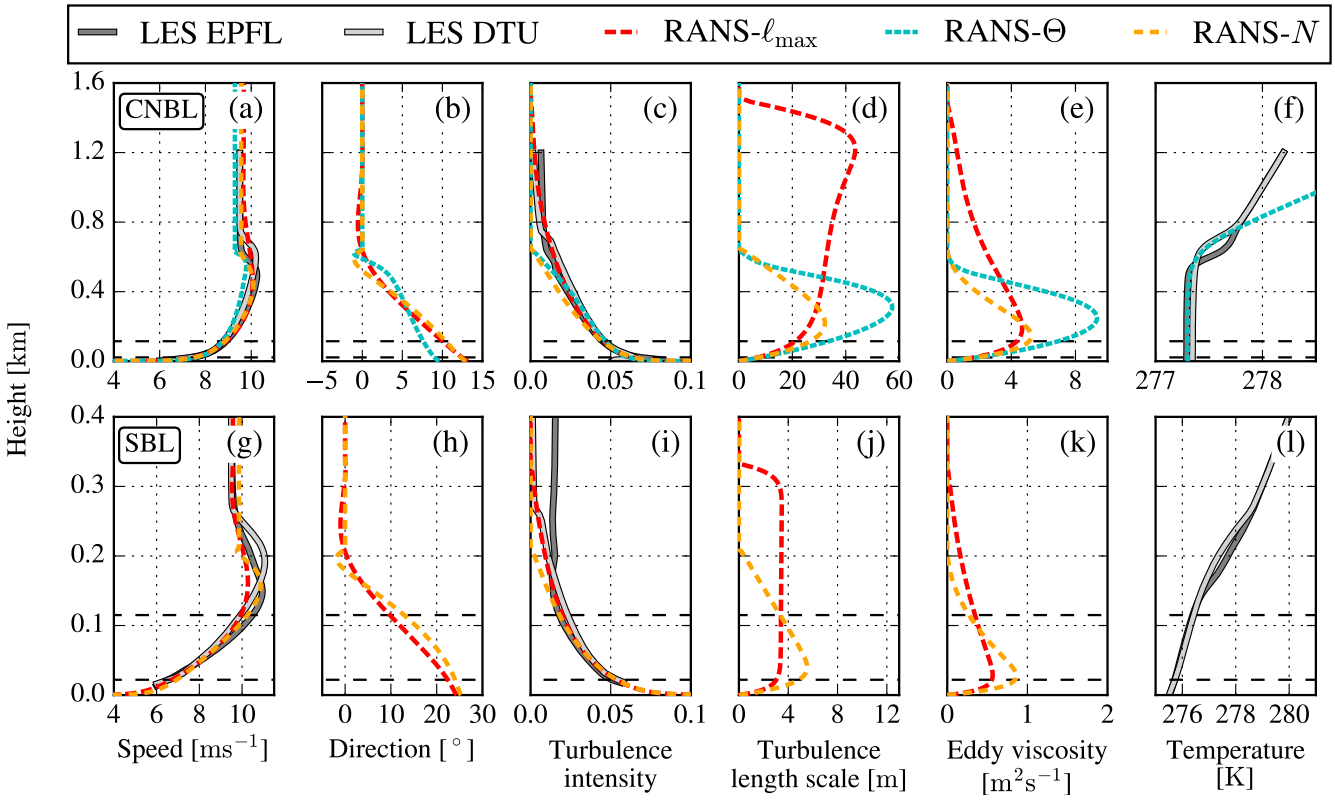

Figure 2. RANS-simulated ABL inflow compared to LES model results from Hodgson et al. (2023), for CNBL **(a-f)** and SBL inflow cases **(g-l)**. Horizontal dashed lines represent rotor swept area of the SWT-2.3-93 wind turbine.

model predicts taller ABLs compared to the RANS-N model. For the SBL case, it is clear that the turbulence length scale in the RANS-ℓ_{max} model is limited to a maximum value of 3.4 m, while the turbulence length scale of the RANS-N model results in a more smooth profile that has a higher value in the surface layer but a lower value around the ABL height. As a result, the profiles of wind speed and direction around the ABL height are more diffused in the RANS-ℓ_{max} model compared to the RANS-N model, which is best visible for the SBL case (Fig. 2g and h) around $z = 0.2$ km. In other words, the RANS-N has more more pronounced Ekman layer. The RANS-N model predicts a lower ABL height compared to the LES models for both ABL cases, but this could be improved by lowering the applied roughness length. The latter is not performed in order to provide a more fair comparison between the RANS-N and RANS-ℓ_{max} models by using the same roughness length. The RANS-Θ model compares well with the LES models for the CNBL case but shows a large turbulence length scale and eddy viscosity compared to the RANS-N due to a zero turbulent buoyancy in the surface layer (Fig. 2d and e). The RANS-Θ model is not applied to the SBL case because the RANS-Θ model cannot represent an SBL nor a shallow CNBL, as discussed in Sect. A.

https://doi.org/10.5194/wes-2024-23
Preprint. Discussion started: 19 March 2024

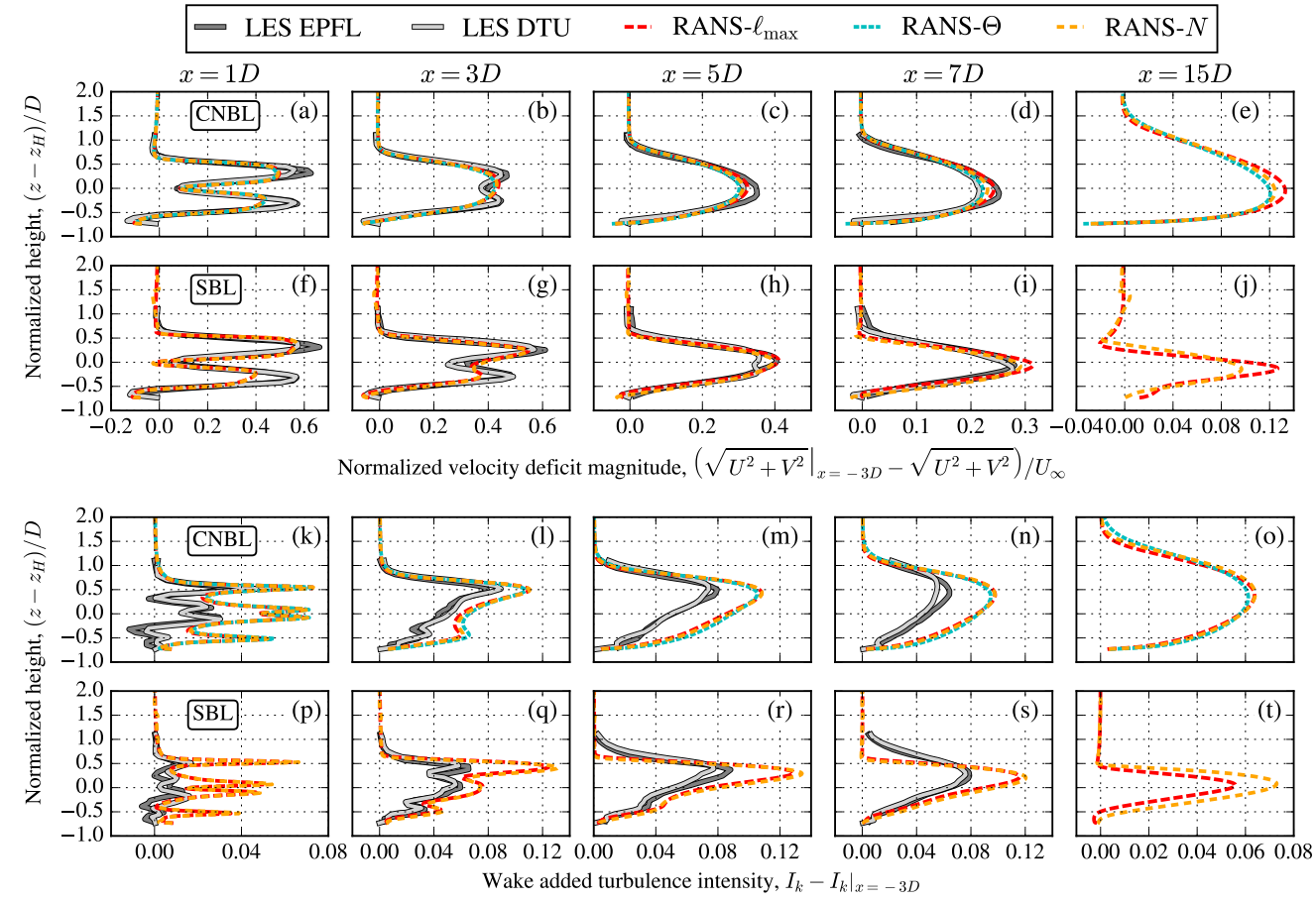

Figure 3. RANS-simulated wake velocity deficit **(a-j)** and wake added TI **(k-t)** compared to LES model results from (Hodgson et al., 2023), for the CNBL **(a-e, k-o)** and SBL inflow cases **(f-j, p-t)**.

The RANS inflow models are applied to single turbine wake simulations and the results of velocity deficit magnitude and wake added turbulence intensity are compared with results from two LES models of Hodgson et al. (2023) in Fig. 3. The wake results are normalized by the results at $x = -3D$ following the LES data. The RANS-Θ model is only applied to the CNBL case and not the SBL case because the model cannot represent a shallow ABL, as discussed in Sect. A. The CNBL case shows that all three RANS inflow models predict similar velocity deficits that follow the trends of the LES models (Fig. 3b-d). The differences between the RANS and LES models in the near wake at $x = 1D$ (Fig. 3a) are expected, following a previous study (van der Laan et al., 2015c). The difference in velocity deficit between the RANS and LES models for the SBL case are larger than the CNBL case. The largest difference between the RANS-$\ell_{\max}$ and RANS-N models is observed at the far wake

https://doi.org/10.5194/wes-2024-23
Preprint. Discussion started: 19 March 2024

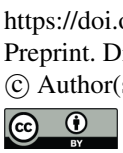

eawe european academy of wind energy
Open Access WIND ENERGY SCIENCE DISCUSSIONS

at $x = 25D$, for the SBL case, where RANS-$\ell_{\max}$ model does not allow the turbine wake to recover vertically with respect to the RANS-N model due to the global length scale limiter. A future study is needed to validate the results of RANS-N model in the far wake.

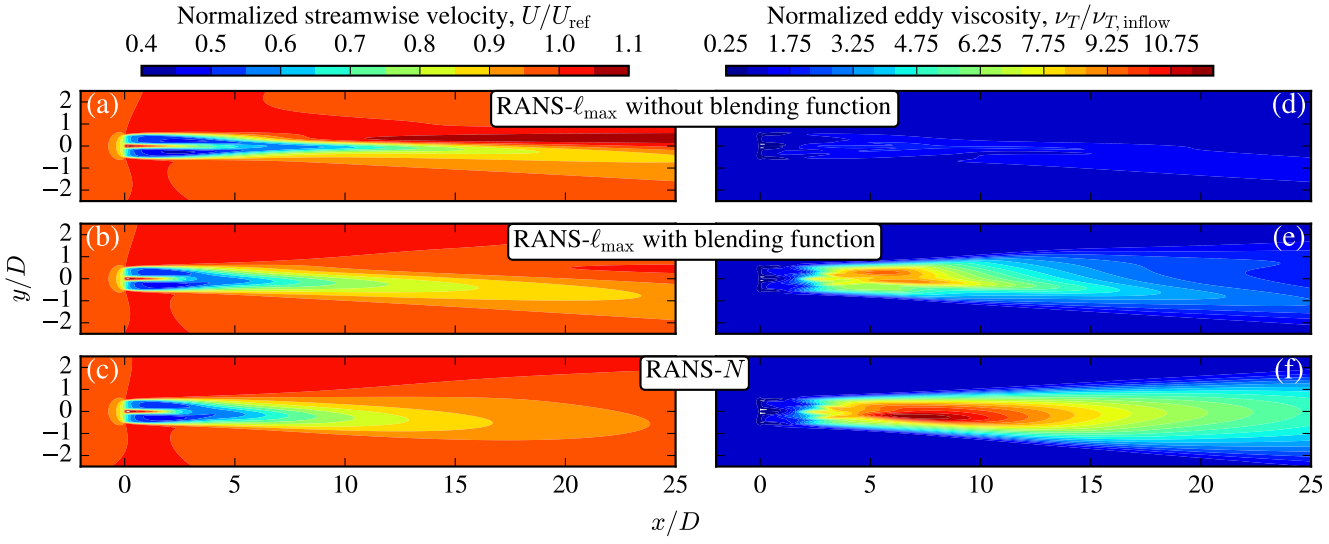

Figure 4. Hub height contours of normalized streamwise velocity **(a-c)** and wake eddy viscosity normalized by inflow eddy viscosity **(d-f)** for SBL case. RANS-$\ell_{\max}$ model without blending function of Eq. (6) **(a, d)**, RANS-$\ell_{\max}$ model with blending function of Eq. (6) **(b, e)** and RANS-N model **(c, f)**.

The RANS-N model results of the SBL single wake case shows a small speed up around the ABL height $(z - z_H)/D \approx 1.4$ at $x = 1D$ (Fig. 3f), which grows further downstream (Fig. 3g-j). This is a numerical issue associated with the low eddy viscosity at the ABL height that can also occur with the other RANS inflow models, especially when they are applied to a large wind farm (van der Laan et al., 2023b). A possible solution is an additional damping momentum source, which is planned to be further investigated in future work.

None of the RANS models are able to predict the wake added turbulence intensity compared to LES (Fig. 3k-t) because of the applied isotropic Boussinesq hypothesis. However, the RANS models do not need a good prediction of wake added turbulence intensity in order to predict a realistic velocity deficit because the wake recovery is dictated by the divergence of the shear stresses (van der Laan et al., 2023a); the latter can be well modeled by the isotropic Boussinesq hypothesis and a variable C_μ (for example through f_P),

Contours of the steamwise velocity and eddy viscosity at hub height of the SBL single wake case are shown in Fig. 4 for the RANS-N and RANS-$\ell_{\max}$ models. Two results of the RANS-$\ell_{\max}$ model are shown, one with and one without the blending function of Eq. (6) that is used to switch off the global turbulence length scale limiter in the wake region (identified

https://doi.org/10.5194/wes-2024-23
Preprint. Discussion started: 19 March 2024

eawe european academy of wind energy
Open Access WIND ENERGY SCIENCE DISCUSSIONS

by the f_P function). Without Eq. (6), the eddy viscosity does not increase significantly because of the global turbulence length scale limiter (Fig. 4d), which delays the recovery of the streamwise velocity deficit and shows a speed up region in far wake (Fig. 4a). When Eq. (6) is included, the eddy viscosity can increase downstream but it quickly returns to the ambient eddy viscosity in the region where the f_P is close to one (Fig. 4e). The RANS-N model does not limit the turbulence length as the RANS-$\ell_{\max}$ model, which results in a smoothly increasing (up to $x = 10D$) and decreasing eddy viscosity (Fig. 4f). As a result, a more smooth far wake velocity deficit is obtained by the RANS-N model (Fig. 4c), which explains the difference between the RANS-$\ell_{\max}$ and RANS-N models at $x = 25D$ shown in Fig. 3j.

5 Conclusions

A new RANS inflow model of the neutral and stable ABL is proposed and compared with two existing RANS inflow models for CNBL and SBL cases based on LES model results. The proposed inflow (RANS-N) model does not require a global length scale limiter or prior knowledge of temperature profile by the use of simple turbulent buoyancy expression based on a constant Brunt-Väisälä frequency. The RANS-N model compares well with LES-predicted profiles of wind speed and turbulence intensity. The simplicity of the RANS-N model results in a reduced parameter space consisting of only two non-dimensional numbers, the surface Rossby number and the Zilintinkevich number. The three RANS inflow models are applied to single wind turbine wakes for the same ABL cases and their simulated velocity deficit compares well with results from LES for the CNBL case. The present study has shown that the proposed RANS-N model is better suited to simulate the effect of a shallow SBL on a wind turbine wake, than the existing state-of-the-art RANS-$\ell_{\max}$ (Apsley and Castro, 1997) and RANS-θ (van der Laan et al., 2023b) models. On the other hand, the interaction of a shallow ABL and a turbine wake in RANS can lead to small numerical wiggles, which grow with downstream distance and needs further investigation.

Appendix A: Double ABL height problem of the RANS-Θ inflow model

The RANS-Θ model can predict a double ABL height if a strange combination of the input parameters is chosen. For example, for a shallow ABL one could set a low z_i, but if the chosen inversion strength is not strong enough then the effective ABL height can occur above the inversion height, $z > z_i$. An example of this issue is shown in Fig. A1, where the RANS-Θ model is employed for $(G, f_c, z_0, z_i, d\Theta/dz|_c) = (10\ \text{m},\ 10^{-4}\ \text{s}^{-1},\ 10^{-4}\ \text{m},\ 100\ \text{m},\ 0.1\ \text{Km}^{-1})$ and three different combinations of z_T/z_i. The standard value ($z_T/z_i = 0.2$) results in the double height problem, which creates an inflection point in the wind speed profile (Fig. A1a) at $z \approx 0.08$ km. When the smoothing is increased by setting larger values of z_T/z_i, then the double ABL height is less visible and the model behaves as the RANS-N model since the temperature gradient approaches a constant value.

One could extend the RANS-Θ model by adding a surface layer temperature gradient, $d\Theta/dz|_s$:

$$\frac{d\Theta}{dz} = \frac{1}{2}\left[1+\tanh\left(\frac{1-z/z_i}{z_T/z_i}\right)\right]\left.\frac{d\Theta}{dz}\right|_s + \frac{1}{2}\left[1+\tanh\left(\frac{z/z_i-1}{z_T/z_i}\right)\right]\left.\frac{d\Theta}{dz}\right|_c, \tag{A1}$$

https://doi.org/10.5194/wes-2024-23
Preprint. Discussion started: 19 March 2024

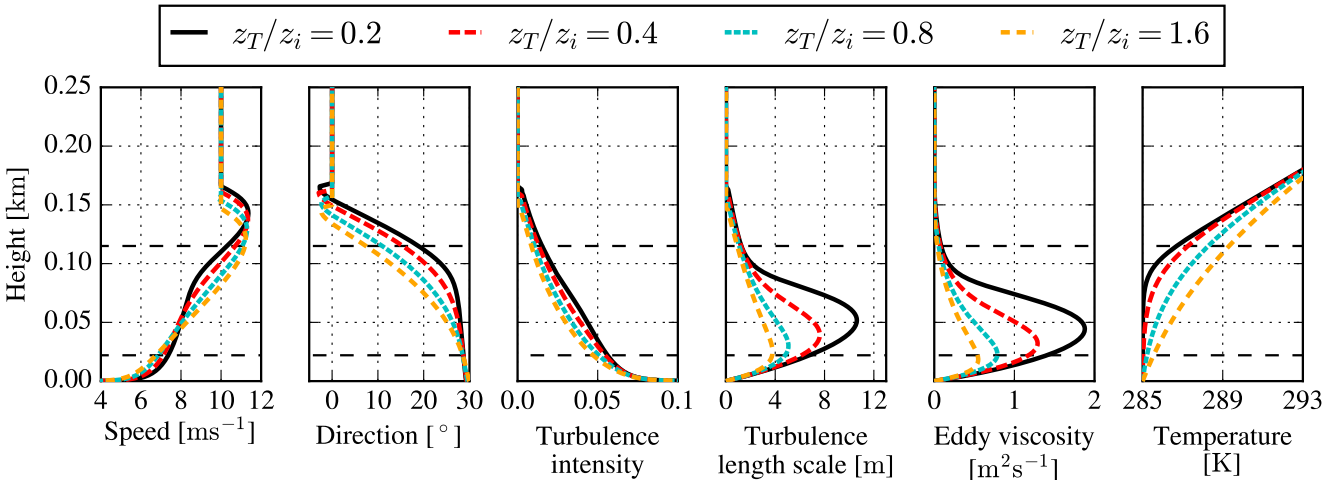

Figure A1. ABL inflow simulated with the RANS-Θ model for different values z_T/z_i. Horizontal dashed lines represent rotor swept area of the SWT-2.3-93 wind turbine.

which can reduce the problem with double ABL heights for a shallow and stable ABL using a positive surface layer gradient. However, the user can still obtain a double ABL height if $d\Theta/dz|_s$ is not strong enough, and for a too strong $d\Theta/dz|_s$, the model can produce a lower ABL height than intended. One could also employ a prescribed temperature gradient profile from a higher fidelity model as LES; however, a smooth wind speed speed profile is not guaranteed. In the present work, we do not use Eq. (A1) but rather adapt the original formulation (van der Laan et al., 2023b).

Appendix B: Grid refinement study of the RANS-N inflow model applied to the SBL single wake case

The grid sensitivity of the proposed RANS-N inflow model applied to the single wake SBL case is depicted in Fig. B1. Three coarser grids are employed compared to the results presented in the main body of the article, which leads to four different grid sizes in the domain around the turbine, Δ: $D/4$, $D/8$, $D/16$ and $D/32$, which correspond to total cell counts of 0.786, 2.65, 8.91 and 37.7 million, respectively. Figure B1a shows the rotor integrated streamwise velocity normalized by the freestream and also includes a Richardson Extrapolated (RE) value following the mixed order grid convergence analysis from Roy (2003). The corresponding discretization error is plotted in Figure B1b and indicates that a grid spacing of $D/8$ results in an error less than 1%, at a downstream distance of $8.5D$ and beyond. Such an error is acceptable for the application of RANS wind farm simulations of modern offshore wind farms, where the typical turbine inter spacing is around $7-10D$.

Code and data availability. The numerical results are generated with proprietary software, although the data presented can be made available by contacting the corresponding author.

https://doi.org/10.5194/wes-2024-23
Preprint. Discussion started: 19 March 2024

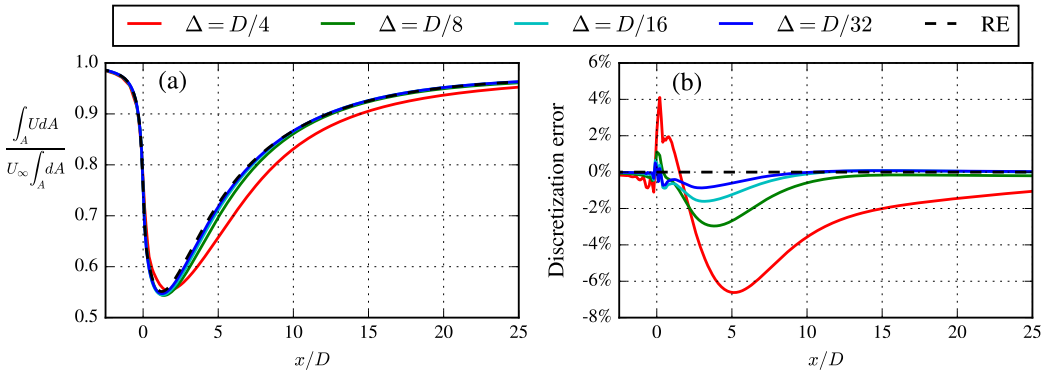

Figure B1. RANS wake velocity integrated, integrated over a fictitious rotor area **(a)** and corresponding discretization error **(b)** simulated by the RANS-N model, for different grid resolutions, for the SBL inflow case.

Author contributions. MPVDL has developed the new ABL inflow model, drafted the article and produced the figures. AD has improved the numerical stability of the numerical simulations. All authors contributed to discussion of the new model, the methodology and finalization of the paper.

Competing interests. The authors declare that they have no conflict of interest.

Financial support. This work has been partially supported by the MERIDIONAL project, which receives funding from the European Union's Horizon Europe Programme under the grant agreement No. 101084216. In addition, this work has also been co-financed by Equinor ASA.

Acknowledgements. We also gratefully acknowledge the computational and data resources provided on the Sophia HPC Cluster at the Technical University of Denmark, DOI: 10.57940/FAFC-6M81.

https://doi.org/10.5194/wes-2024-23
Preprint. Discussion started: 19 March 2024

eawe european academy of wind energy
Open Access WIND ENERGY SCIENCE DISCUSSIONS

References

Apsley, D. D. and Castro, I. P.: A limited-length-scale k-ε model for the neutral and stably-stratified atmospheric boundary layer, Boundary-Layer Meteorology, 83, 75–98, https://doi.org/10.1023/A:1000252210512, 1997.

Avila, M., Gargallo-Peiró, A., and Folch, A.: A CFD framework for offshore and onshore wind farm simulation, Journal of Physics: Conference Series, 854, 012 002, https://doi.org/10.1088/1742-6596/854/1/012002, 2017.

Baungaard, M., Wallin, S., van der Laan, M. P., and Kelly, M.: Wind turbine wake simulation with explicit algebraic Reynolds stress modeling, Wind Energy Science, 7, 1975–2002, https://doi.org/10.5194/wes-7-1975-2022, 2022.

Baungaard, M., van der Laan, M. P., Kelly, M., and Hodgson, E.: Simulation of a conventionally neutral boundary layer with two-equation URANS, Submitted to Torque, 2024.

Beare, R. J., Macvean, M. K., Holtslag, A. A. M., Cuxart, J., Esau, I., Golaz, J.-C., Jimenez, M. A., Khairoutdinov, M., Kosovic, B., Lewellen, D., Lund, T. S., Lundquist, Julie K. andMccabe, A., Moene, A. F., Noh, Y., Raasch, S., and Sullivan, P.: An Intercomparison of Large-Eddy Simulations of the Stable Boundary Layer, Boundary-Layer Meteorology, 2, 247–272, https://doi.org/https://doi.org/10.1007/s10546-004-2820-6, 2006.

Calaf, M., Meneveau, C., and Meyers, J.: Large eddy simulation study of fully developed wind-turbine array boundary layers, Physics of Fluids, 22, 015 110, https://doi.org/10.1063/1.3291077, 2010.

Chougule, A., Mann, J., Kelly, M., and Larsen, G.: Modeling Atmospheric Turbulence via Rapid Distortion Theory: Spectral Tensor of Velocity and Buoyancy, Journal of the Atmospheric Sciences, 74, 949–974, https://doi.org/10.1175/JAS-D-16-0215.1, 2017.

DTU Wind and Energy Systems: PyWakeEllipSys v4.0, https://topfarm.pages.windenergy.dtu.dk/cuttingedge/pywake/pywake_ellipsys/, 2024.

Ekman, V. W.: On the influence of the earth's rotation on ocean-currents, Arkiv Mat. Astron. Fysik, 2, 1905.

Ellison, T. H.: Atmospheric Turbulence in Surveys of mechanics, Cambridge University Press, Cambridge, U. K., 1956.

Hansen, K. S., Barthelmie, R. J., Jensen, L. E., and Sommer, A.: The impact of turbulence intensity and atmospheric stability on power deficits due to wind turbine wakes at Horns Rev wind farm, Wind Energy, 15, 183–196, https://doi.org/https://doi.org/10.1002/we.512, 2012.

Hodgson, E. L., Souaiby, M., Troldborg, N., Porté-Agel, F., and Andersen, S. J.: Cross-code verification of non-neutral ABL and single wind turbine wake modelling in LES, Journal of Physics: Conference Series, 2505, 012 009, https://doi.org/10.1088/1742-6596/2505/1/012009, 2023.

Kelly, M. C., Cersosimo, R. A., and Berg, J.: A universal wind profile for the inversion-capped neutral atmospheric boundary layer, Quarterly Journal of the Royal Meteorological Society, 145, 982–992, https://doi.org/10.1002/qj.3472, 2019.

Koblitz, T., Bechmann, A., Sogachev, A., Sørensen, N., and Réthoré, P.-E.: Computational Fluid Dynamics model of stratified atmospheric boundary-layer flow, Wind Energy, 18, 75–89, https://doi.org/10.1002/we.1684, 2015.

Michelsen, J. A.: Basis3D - a platform for development of multiblock PDE solvers., Tech. Rep. AFM 92-05, Technical University of Denmark, Lyngby, Denmark, 1992.

Monin, A. S. and Obukhov, A. M.: Basic laws of turbulent mixing in the surface layer of the atmosphere, Tr. Akad. Nauk. SSSR Geophiz. Inst., 24, 163–187, 1954.

Nilsson, K., Ivanell, S., Hansen, K. S., Mikkelsen, R., Sørensen, J. N., Breton, S.-P., and Henningson, D.: Large-eddy simulations of the Lillgrund wind farm, Wind Energy, 18, 449–467, https://doi.org/https://doi.org/10.1002/we.1707, 2015.

https://doi.org/10.5194/wes-2024-23
Preprint. Discussion started: 19 March 2024

Politis, E. S., Prospathopoulos, J., Cabezon, D., Hansen, K. S., Chaviaropoulos, P. K., and Barthelmie, R. J.: Modeling wake effects in large wind farms in complex terrain: the problem, the methods and the issues, Wind Energy, 15, 161–182, https://doi.org/https://doi.org/10.1002/we.481, 2012.

Porté-Agel, F., Bastankhah, M., and Shamsoddin, S.: Wind-Turbine and Wind-Farm Flows: A Review, Boundary-Layer Meteorology, 174, 1–59, https://doi.org/https://doi.org/10.1007/s10546-019-00473-0, 2020.

Réthoré, P.-E., van der Laan, M. P., Troldborg, N., Zahle, F., and Sørensen, N. N.: Verification and validation of an actuator disc model, Wind Energy, 17, 919–937, https://doi.org/10.1002/we.1607, 2014.

Roy, C. J.: Grid Convergence Error Analysis for Mixed-Order Numerical Schemes, AIAA Journal, 41, 595–604, https://doi.org/10.2514/2.2013, 2003.

Sogachev, A., Kelly, M., and Leclerc, M. Y.: Consistent Two-Equation Closure Modelling for Atmospheric Research: Buoyancy and Vegetation Implementations, Boundary-Layer Meteorology, 145, 307–327, https://doi.org/10.1007/s10546-012-9726-5, 2012.

Sørensen, J. N., Nilsson, K., Ivanell, S., Asmuth, H., and Mikkelsen, R. F.: Analytical body forces in numerical actuator disc model of wind turbines, Renewable Energy, 147, 2259, https://doi.org/https://doi.org/10.1016/j.renene.2019.09.134, 2020.

Sørensen, N. N.: General purpose flow solver applied to flow over hills, Ph.D. thesis, Risø National Laboratory, Roskilde, Denmark, 1994.

Sørensen, N. N., Bechmann, A., Johansen, J., Myllerup, L., Botha, P., Vinther, S., and Nielsen, B. S.: Identification of severe wind conditions using a Reynolds Averaged Navier-Stokes solver, Journal of Physics: Conference series, 75, 1–13, https://doi.org/10.1088/1742-6596/75/1/012053, 2007.

van der Laan, M. P. and Sørensen, N. N.: A 1D version of EllipSys, Tech. Rep. DTU Wind Energy E-0141, Technical University of Denmark, 2017.

van der Laan, M. P., Hansen, K. S., Sørensen, N. N., and Réthoré, P.-E.: Predicting wind farm wake interaction with RANS: an investigation of the Coriolis force, Journal of Physics: Conference Series, 625, 012 026, https://doi.org/10.1088/1742-6596/625/1/012026, 2015a.

van der Laan, M. P., Sørensen, N. N., Réthoré, P.-E., Mann, J., Kelly, M. C., and Troldborg, N.: The k-ε-f_P model applied to double wind turbine wakes using different actuator disk force methods, Wind Energy, 18, 2223–2240, https://doi.org/10.1002/we.1816, 2015b.

van der Laan, M. P., Sørensen, N. N., Réthoré, P.-E., Mann, J., Kelly, M. C., Troldborg, N., Schepers, J. G., and Machefaux, E.: An improved k-ε model applied to a wind turbine wake in atmospheric turbulence, Wind Energy, 18, 889–907, https://doi.org/10.1002/we.1736, 2015c.

van der Laan, M. P., Andersen, S. J., and Réthoré, P.-E.: Brief communication: Wind-speed-independent actuator disk control for faster annual energy production calculations of wind farms using computational fluid dynamics, Wind Energy Science, 4, 645–651, https://doi.org/10.5194/wes-4-645-2019, 2019.

van der Laan, M. P., Kelly, M., Floors, R., and Peña, A.: Rossby number similarity of an atmospheric RANS model using limited-length-scale turbulence closures extended to unstable stratification, Wind Energy Science, 5, 355–374, https://doi.org/10.5194/wes-5-355-2020, 2020.

van der Laan, M. P., Andersen, S. J., Réthoré, P.-E., Baungaard, M., Sørensen, J. N., and Troldborg, N.: Faster wind farm AEP calculations with CFD using a generalized wind turbine model, Journal of Physics: Conference Series, 2265, 022 030, https://doi.org/10.1088/1742-6596/2265/2/022030, 2022.

van der Laan, M. P., Baungaard, M., and Kelly, M.: Brief communication: A clarification of wake recovery mechanisms, Wind Energy Science, 8, 247–254, https://doi.org/10.5194/wes-8-247-2023, 2023a.

van der Laan, M. P., García-Santiago, O., Kelly, M., Meyer Forsting, A., Dubreuil-Boisclair, C., Sponheim Seim, K., Imberger, M., Peña, A., Sørensen, N. N., and Réthoré, P.-E.: A new RANS-based wind farm parameterization and inflow model for wind farm cluster modeling, Wind Energy Science, 8, 819–848, https://doi.org/10.5194/wes-8-819-2023, 2023b.